Available online at www.sciencedirect.com

ScienceDirect

Ceramics International 40 (2014) 531–540

CERAMICS INTERNATIONAL

www.elsevier.com/locate/ceramint

In-situ formation of carbon nanotubes in pyrolytic carbon–silicon nitride composite ceramics

Xingmin Liu[a,b], Xiaowei Yin[b,*], Guopeng Zheng[b], Ye Liu[b], Luo Kong[b], Quan Li[b], Xiaowen Yuan[a,c]

[a]*State Key Laboratory of Solidification processing, Northwestern Polytechnical University, West Youyi Rd. No. 127, Xi'an, Shaanxi 710072, China*

[b]*Science and Technology on Thermostructure Composite Materials Laboratory, Northwestern Polytechnical University, West Youyi Rd. No. 127, Xi'an, Shaanxi 710072, China*

[c]*Department of Mechanical Engineering, The University of Auckland, 20 Symonds Street, Auckland, New Zealand*

Received 26 April 2013; received in revised form 27 May 2013; accepted 4 June 2013
Available online 18 June 2013

Abstract

Carbon nanotube reinforced pyrolytic carbon/silicon nitride (CNT-PyC/Si_3N_4) composite ceramics were fabricated through in-situ growth of CNTs in PyC–Si_3N_4 ceramics by precursor infiltration and pyrolysis. CNTs were in-situ formed by the addition of nano-sized Ni into phenolic resin and Si_3N_4 powder blend, and the content of CNTs increased with the increase of Ni content. Due to the formation of CNTs in the inter-particle pores of CNTs/PyC–Si_3N_4 ceramic, the PyC wrapped Si_3N_4 particles were bridged by CNTs, which led to the increase of electrical conductivity. Different from the previously reported PyC–Si_3N_4 ceramics fabricated by chemical vapor infiltration (CVI), the PyC–Si_3N_4 ceramics exhibited a shielding mechanism dominated by absorption. Compared to PyC–Si_3N_4 ceramics prepared with same procedure, the shielding effectiveness of CNTs-PyC/Si_3N_4 increased significantly with the formation of CNTs. With the increase of CNT content, the shielding effectiveness of CNTs/PyC–Si_3N_4 ceramics increased from 25.5 to 43.6 dB, in which the absorption shielding effectiveness increased from 15 to 30 dB over the frequency range of 8.2–12.4 GHz.

Keywords: Carbon nanotubes; Ceramics; Electromagnetic shielding; Microstructure

1. Introduction

Recently, lots of researches have been carried out to investigate the electromagnetic (EM) shielding for the purpose of protecting environment and sensitive devices from electromagnetic interference (EMI) [1–6]. A traditional way to eliminate EMI is to use metal as a shielding material [7,8]. However, the shielding mechanism of metal materials is mainly reflected due to the mobile charge carriers and high electrical conductivity (σ). The reflected EM wave from shielding material could also interfere with the devices. As a comparison, ceramic is more suitable to be used as shielding material than metal in harsh environment, which is attributed to the unique properties of ceramics such as low density, good oxidation resistance, relatively high hardness, thermal–chemical corrosion resistance, good machinability, high creep resistance, and high thermal shock resistance [9–13]. Compared with ceramics, carbon possesses comparatively high electrical conductivity, low density, improved EM absorption property, and good environment stability [14], so carbon and ceramic hybrid materials are promisingly used as shielding material in harsh environment instead of ceramic. In our previous work, the EM shielding properties of pyrolytic carbon reinforced silicon nitride (PyC–Si_3N_4) composite ceramics fabricated by chemical vapor infiltration (CVI)[15] and precursor infiltration pyrolysis (PIP)[16] methods have been investigated. It was found that the high electrical conductivity of PyC–Si_3N_4 ceramic fabricated by the CVI method always led to a relatively high reflection shielding effectiveness (SE_R) compared with absorption shielding effectiveness (SE_A).

*Corresponding author. Tel.: +86 29 88494947; fax: +86 29 88494620.
E-mail addresses: yinxw@nwpu.edu.cn, xwyin2001@yahoo.com.cn (X. Yin)

0272-8842/$ - see front matter © 2013 Elsevier Ltd and Techna Group S.r.l. All rights reserved.
http://dx.doi.org/10.1016/j.ceramint.2013.06.035

Table 1
PyC content, density, porosity, sample thickness, electrical conductivity and EMI SE of PyC/Si_3N_4 composite ceramic fabricated by CVI and PIP methods.

Fabrication process	PyC content (vol%)	SE_T (dB)	SE_A (dB)	SE_R (dB)	Sample thickness (mm)	Porosity (%)	Density (g/cm^3)	Electrical conductivity (S/m)
CVI	12.1	26.3	5.3	21.0	0.7	31.7	1.99	2.6×10^4
PIP	4.0	13.0	8.0	5.0	2.0	10.2	2.70	4.2

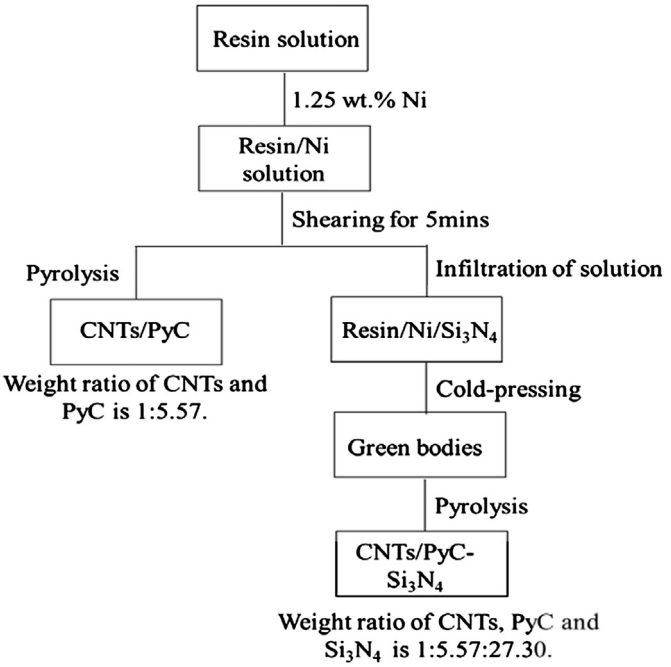

Fig. 1. Schematic illustration of experimental procedure.

The PyC–Si_3N_4 ceramics fabricated by the PIP method possessed a relatively high SE_A compared to SE_R owing to the lower electrical conductivity. However, the overall shielding property of the material was relatively low (Table 1). Usually, a total shielding effectiveness (SE_T) of 30 dB, corresponding to 99.9% attenuation of the EMI radiation, is considered as an adequate level of shielding for many applications [17]. Carbon nanotubes (CNTs) as an excellent EM wave absorber (CNTs) have been widely used in polymer-based materials for EMI shielding [18–20]. However, the EMI SE of CNT reinforced Si_3N_4 ceramics has not been reported due to the difficulties in dispersing CNTs, which are apt to agglomerate, and in avoiding the damage on CNTs at high fabrication temperatures [21].

In the present work, PyC–Si_3N_4 composite ceramics reinforced by CNTs (CNTs/PyC–Si_3N_4) were fabricated through in-situ growth of CNTs by pyrolysis of phenolic resin containing Ni catalyst with the PIP method. The aim of this work is to fabricate a novel Si_3N_4 based shielding composite ceramic which possesses higher SE_A and low SE_R. In this work, the effects of Ni loadings on the content of CNTs, on the microstructure of PyC–Si_3N_4, on the electrical conductivity and EMI SE of the as-prepared materials are investigated, respectively.

2. Experimental procedure

2.1. Preparation of CNTs-PyC materials

Fig. 1 shows the schematic illustration of experimental procedure. Phenolic resin (PF 2313, purity > 96.5% Xi'an resin factory, Xi'an, China), ethanol and hexamethylenetetramine ($C_6H_{12}N_4$) which acts as a curing agent, were mixed by a weight ratio of 10:10:1, and nano-sized Ni particles (mean particle size 50 nm, purity > 99.9%) were prepared by a weight ratio of 0, 0.25, 0.50, 0.75 and 1.25 wt% of phenolic resin, respectively. When the phenolic resin was uniformly dissolved in ethanol, the Ni powders were added into phenolic resin solution, and then the different Ni contained phenolic resin solution samples were sheared with an emulsifier at a speed of 7000 r/min for 5 min. After dried for 48 h at 80 °C, the phenolic resin specimens with different catalyst were pyrolysed at 1000 °C for 2 h. The heating rate was 5 °C/min. In this experiment, the formation of CNTs could lead to the increase in carbon yield of phenolic resin. To vary the carbon yield of phenolic resin with different Ni catalyst, the carbon yield is defined as follows:

$$\text{Carbon yield } \% = \frac{W_{CP}}{W_{PR}} \times 100 \quad (1)$$

where W_{PR} and W_{CP} are the weight of phenolic resin and carbon phase (PyC or CNTs/PyC) derived from pyrolysis of phenolic resin, respectively.

2.2. Preparation of CNTs/PyC–Si_3N_4 ceramics

Phenolic resin solution with 0–1.25 wt% Ni loadings was infiltrated into Si_3N_4 (mean particle size of 1.2 μm, α-Si_3N_4 > 95%), and the weight ratio of phenolic resin and Si_3N_4 was 3:7. When dried for 48 h at 80 °C, the obtained Si_3N_4 and phenolic resin blend was cold-pressed into green bodies and pyrolyzed in Ar at 1000 °C for 2 h. The heating rate was also 5 °C/min. After pyrolysis, the as-received porous CNTs/PyC–Si_3N_4 ceramics were machined into specimens, which were designated as samples A, B, C, D and E, corresponding to 0, 0.25, 0.5, 0.75 and 1.25 wt% Ni content of phenolic resin in the green bodies, with dimensions of 22.86 mm (length) × 10.16 mm (width) × 2 mm (thickness).

2.3. Compositional and microstructural characterization

X-ray diffraction (XRD) was employed for phase analysis (X'Pert Pro, Philips, Netherlands). INVIN Raman spectroscopy (RMS; Renishaw, UK) was used to characterize the

graphitization degree of CNTs/PyC. The microstructure of the samples was observed by scanning electron microscopy (SEM; S-4700, Hitachi, Tokyo, Japan). Transmission electron microscope (TEM; G-20, FEI-Tecnai, Hillsboro, USA) was employed to characterize the microstructure of CNTs.

2.4. Electrical and EM shielding property characterization

Electrical conductivity was measured by the two-wire method using a current source (Keithley 6220 DC, Ohio, USA). Scattering parameters (*S*-parameters, S_{11} and S_{21}) in 8.2–12.4 GHz were measured by a vector network analyzer (VNA; MS4644A, Anritsu, Kana-gawa, Japan) using the waveguide method. In this work, total shielding properties were assessed by SE_T. SE_R and SE_A were calculated according to the measured reflected (R) and transmitted (T) coefficients:

$$SE_R = -10 \times \log_{10}(1-R) \quad (2)$$

$$SE_A = -10 \times \log_{10}(T/(1-R)) \quad (3)$$

$$SE_T = SE_A + SE_R \quad (4)$$

where R and T are calculated according to

$$R = |S_{11}|^2,\ T = |S_{21}|^2 \quad (5)$$

3. Results and discussion

3.1. Effect of Ni loadings on the content of CNTs in CNTs/PyC

The addition of Ni catalyst could lead to an increase in carbon yield. Fig. 2 displays the TGA and DSC curves of phenolic resin containing 0 and 1.25 wt% Ni catalyst. At the temperatures higher than 130 °C, the weight of the system began to decrease with H_2O molecular evaporating out [22]. When the temperature reached 200 °C, CO_2 and CO were released. According to TGA results, the weight loss mainly

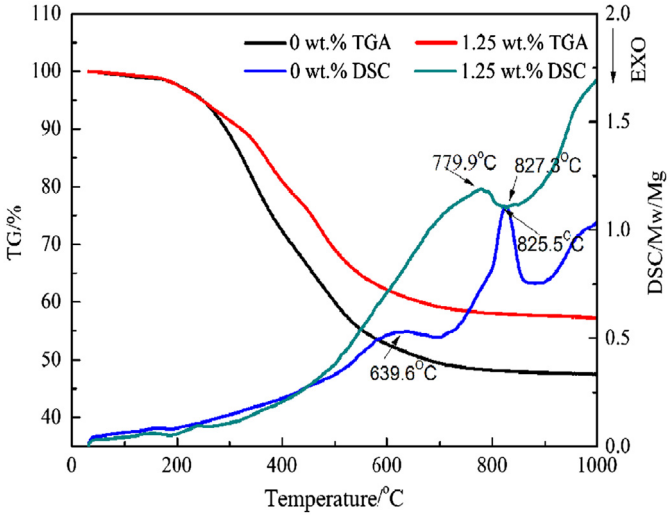

Fig. 2. TGA and DSC curves of phenolic resin containing 0 and 1.25 wt% Ni catalyst.

happened in the temperature range of 300–600 °C. In this stage, gaseous products such as H_2, CH_4, CO_2 and other hydrocarbon gases evaporated out of phenolic resin [22]. With the temperature increasing, the weight loss of phenolic resin increased gradually. At temperatures above 900 °C, the carbonization process has apparently gone to completion. After pyrolysis, phenolic resin exhibited a carbon yield of 47.46 wt%, which increased to 56.00 wt% for phenolic resin containing 1.25 wt% Ni. During the pyrolysis, when the gaseous hydrocarbon evaporating out of phenolic resin passed over Ni catalyst, decomposition of hydrocarbon was achieved on the catalyst surface, and then CNTs were in-situ formed (Fig. 3). Fig. 3(a) and (b) shows the SEM images of PyC and CNTs/PyC derived from pyrolysis of pure phenolic resin and phenolic resin containing 1.25 wt% Ni catalyst. In Fig. 3(b), with the addition of Ni catalyst, plenty of CNTs was in-situ formed. Fig. 3(c) shows the TEM image of a single CNT. The CNTs exhibited apparent burls, indicating a growth mechanism of carbon nanoparticles–nanowires–nanotubes. Similar growth mechanism was reported in the literatures [23,24], in which the CNTs were prepared by floating and detonation-assisted CVD methods. Fig. 3(d) shows HRTEM micrograph of a multi-walled microstructure of CNTs. Table 2 lists the carbon yield of phenolic resin containing 0–1.25 wt% Ni catalyst after pyrolysis at 1000 °C. In Table 2, W_R is the gross residual weight of phenolic resin containing different contents of Ni catalyst and W_{CP} as carbon phase, in which the weight of Ni is subtracted from W_R. When the Ni content varied from 0 to 1.25 wt%, the carbon yield increased from 47.46 to 56.00 wt%, in which content of CNTs increased from 0 to 8.54 wt%.

In Fig. 2, the DSC curve of pure phenolic resin shows two endothermic peaks in the vicinity of 639.6 °C and 828.5 °C. These two peaks are associated with the thermal decomposition of hydrocarbon evaporating out of phenolic resin [25]. Compared with the DSC curve of pure phenolic resin, the weak endothermic peak at 639.6 °C disappeared in that of phenolic resin containing 1.25 wt% Ni, the endothermic peak at 828.5 °C turned smaller in intensity and the corresponding temperature shifted to 778.9 °C, and an exothermic peak appeared at 827.3 °C, which was not observed for the pure resin. With the addition of Ni, the apparent activation energy of decomposition reaction can be obviously reduced while the hydrocarbon decomposition takes place on the catalyst surface [26]. Therefore, the first weak peak at 639.6 °C disappeared and the second peak turned correspondingly weaker due to the addition of Ni catalyst. For synthesizing CNTs, typically, nanometer-size metal particles are required to enable hydrocarbon decomposition at a lower temperature than the spontaneous decomposition temperature of the hydrocarbon [27], so the endothermic peak at 828.5 °C decreased to 778.9 °C with the addition of catalyst. The growth of MWCNT is a graphitization process of amorphous carbon. The graphitization behavior of amorphous carbon mainly consists of two steps: (i) the growth of small graphitic crystallites and (ii) reorientation and merging of the crystallites to form a three-dimensional graphitic order [28]. During this process, the excess free energy of the amorphous state relative to the stable

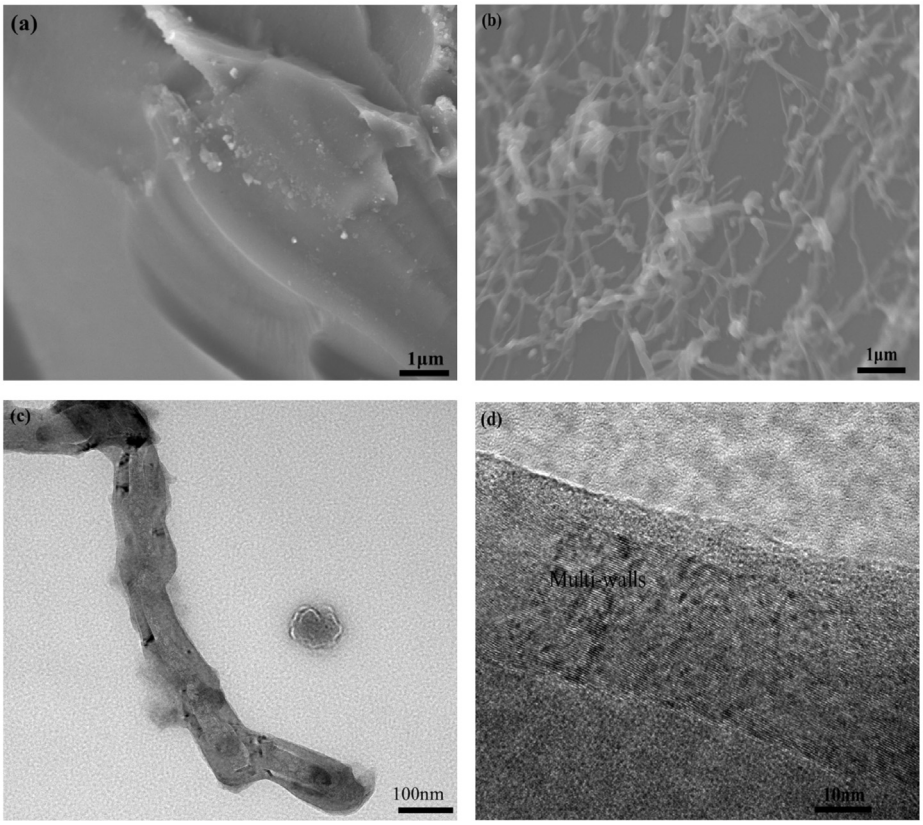

Fig. 3. SEM and TEM images, (a) SEM image of PyC derived from phenolic resin containing 0 wt% Ni catalyst, (b) SEM image of CNTs/PyC derived from phenolic resin containing 1.25 wt% Ni catalyst, (c) TEM image of a single CNT, (d) HRTEM image of CNT.

Table 2
Carbon yield of phenolic resin samples containing 0–1.25 wt% Ni catalyst.

Ni content (wt%) in phenolic resin	0	0.25	0.50	0.75	1.25
W_R (wt%)	47.46	48.28	52.00	56.49	57.25
W_{CP} (wt%)	47.46	48.03	51.50	55.74	56.00

crystalline phase is instantaneously released [29,30], leading to the appearance of the exothermic peak for phenolic resin containing 1.25 wt% Ni catalyst.

Fig. 4 shows the XRD pattern of PyC and CNTs/PyC samples derived from pyrolysis of phenolic resin containing 0–1.25 wt% Ni. An obvious peak of C(002) plane from CNTs at 2θ of 26.5° [20] appeared with the addition of Ni catalyst. With the increase in content of Ni catalyst, the intensity of the carbon peak increased gradually. Obviously, the formation of CNTs could lead to an improvement in the graphitization degree of the CNTs/PyC, and the graphitization degree increased with the increase of CNT content. It is known that higher intensity of C(002) peak is indicative of a more improved graphitic degree [31]. Therefore, with the increase of Ni content, the content of CNTs formed in CNTs/PyC increased gradually.

The Raman spectra of PyC derived from phenolic resin and CNTs/PyC samples derived from phenolic resin containing 0.25–1.25wt% Ni exhibited D-peak at around 1356 cm^{-1} associated with defects and disorder degree, and G-band at

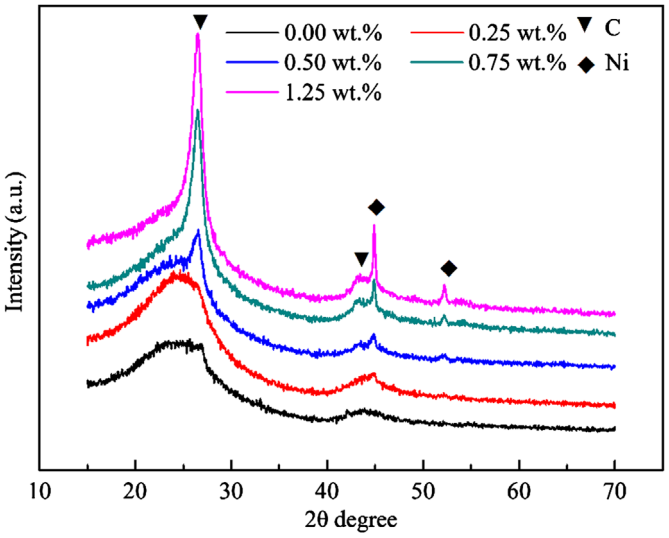

Fig. 4. XRD pattern of PyC and CNTs/PyC derived from pyrolysis of phenolic resin containing 0, 0.25, 0.5, 0.75 and 1.25 wt% Ni catalyst.

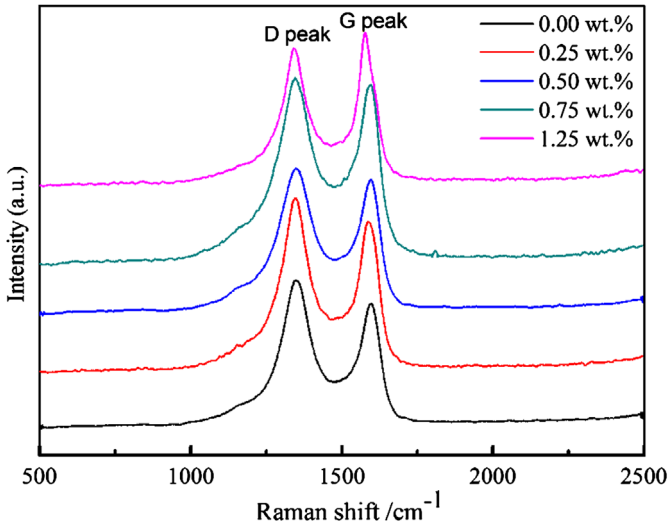

Fig. 5. Raman spectrum of PyC and CNTs/PyC derived from pyrolysis of phenolic resin containing 0, 0.25, 0.5, 0.75 and 1.25 wt% Ni catalyst.

around 1582 cm^{-1} corresponding to the signal from graphite (Fig. 5). The graphitization degree of PyC and CNTs/PyC samples can be determined by the I_D:I_G ratio. The lower the D:G ratio is, the higher graphitization degree of the samples. The PyC sample had a D:G ratio of 1.156, while the CNTs/PyC samples derived from phenolic resin containing 0.25–1.25wt% Ni attained D:G ratios of 1.136, 1.070, 1.031 and 0.912, respectively. The Raman spectra indicate that the content of CNTs increased with the increase of Ni content in the phenolic resin, which is consistent with the XRD patterns.

3.2. Formation of CNTs in Si_3N_4 ceramics

When the effect of Ni loadings on the content of CNTs was obtained, CNTs were in situ formed by infiltration and pyrolysis of phenolic resin containing Ni catalyst in Si_3N_4. After pyrolysis at 1000 °C, CNTs/PyC–Si_3N_4 composite ceramics were obtained. Fig. 6(a)–(e) shows the SEM images of CNTs/PyC–Si_3N_4 ceramic derived from pyrolysis of green bodies containing 0–1.25 wt% Ni in phenolic resin. PyC was uniformly distributed among Si_3N_4 particles in sample A (Fig. 6(a)). Owing to the addition of Ni catalyst in samples B–E (Fig. 6(b)–(e)), CNTs were in-situ formed in the pores of PyC–Si_3N_4 ceramic. With the increase of Ni content, the content of CNTs increased gradually, which is consistent with the variation in CNTs/PyC. Fig. 6(f) exhibits the TEM image of CNT formed in CNTs/PyC–Si_3N_4. The black particles wrapped in CNTs were Ni catalyst with a particle size of 40–60 nm. In the TEM image, obvious burl of CNT appeared between Ni particles, which exhibited the same growth mechanism as the one in CNTs/PyC. Fig. 7 shows the XRD pattern of PyC–Si_3N_4 ceramic (sample A) and CNTs/PyC–Si_3N_4 ceramic (sample E). Compared with sample A, the intensity of weak carbon peak at 2θ of 20–30° of sample E increased slightly. Since the intensity of Si_3N_4 peak was highly intense, the carbon peak intensity was correspondingly weakened. Additionally, the weight percentage of CNTs in PyC–Si_3N_4 was less due to the small weight ratio of phenolic resin to Si_3N_4 in the green bodies. The content of CNTs in CNTs/PyC–Si_3N_4 samples derived from pyrolysis of green bodies with phenolic resin containing 0–1.25 wt% Ni catalyst is listed in Table 3.

3.3. Effect of Ni content on electrical conductivity

Fig. 8 shows the electrical conductivity of PyC–Si_3N_4 and CNTs/PyC–Si_3N_4 samples A, B, C, D and E as a function of Ni content increasing from 0 to 1.25 wt% in phenolic resin. The electrical conductivity of the samples increased with the increase in CNT concentration, which varied from 16.6 to 32.1 S/m. Due to the formation of CNTs in the material, the PyC wrapped Si_3N_4 particles were bridged by CNTs. The values of electrical conductivity of Si_3N_4, PyC and CNTs are 10^{-13}, 10 and 10^4 S/m, respectively [32–34]. The electrical conductivity of CNTs is superior to that of PyC. In CNTs/PyC–Si_3N_4 ceramic, the bridging of PyC wrapped Si_3N_4 particles by CNTs provided the paths for the electrical current, leading to the considerable decrease of the resistance. Therefore, the increase in conductivity can be ascribed to the formation of CNTs.

3.4. Effect of Ni content on EMI SE

Shielding mechanisms of conductive shielding material include reflection, absorption and multiple reflections [35–37]. Multiple reflections are the internal reflections between the internal surfaces of the shielding material. When the shielding material is thicker than the skin depth, the multiple reflections are typically ignored. The skin depth is the distance at which the strength of electric field drops to (1/e) of the incident strength. Mathematically, this can be calculated using [36,37]

$$\delta = (\sqrt{\pi f \mu \sigma})^{-1} \quad (6)$$

where δ is the skin depth, f is the frequency, μ is the magnetic permeability (μ=$\mu_o\mu_r$), μ_o is equal to $4\pi \times 10^{-7}$ Hm^{-1}, μ_r is the relative magnetic permeability and σ is the electrical conductivity of the shield. In the calculations, the relative magnetic permeability was assumed to be 1. Fig. 9 illustrates the influence of the composite conductivity on the skin depth of CNTs/PyC–Si_3N_4 composite ceramics. The results show a significant decrease in skin depth with the increase in conductivity. When the electrical conductivity increased from 16.6 to 32.1 S/m, the skin depth decreased from 1.38 to 1.00 mm, which means that the sample with thickness of 2 mm in this work is independent of the influence of multiple reflections. Therefore, the attenuation of EM radiation will be mainly attributed to the shielding by reflection and absorption.

A great deal of interacting mobile charge carriers resulting from higher concentration of CNTs could lead to a higher EMI SE, which has been demonstrated [38,39]. Fig. 10 depicts the EMI SE of CNTs/PyC–Si_3N_4 ceramic samples as a function of frequency in X-band. Compared with SE_T values of sample A, SE_T values of samples B, C, D and E increased significantly

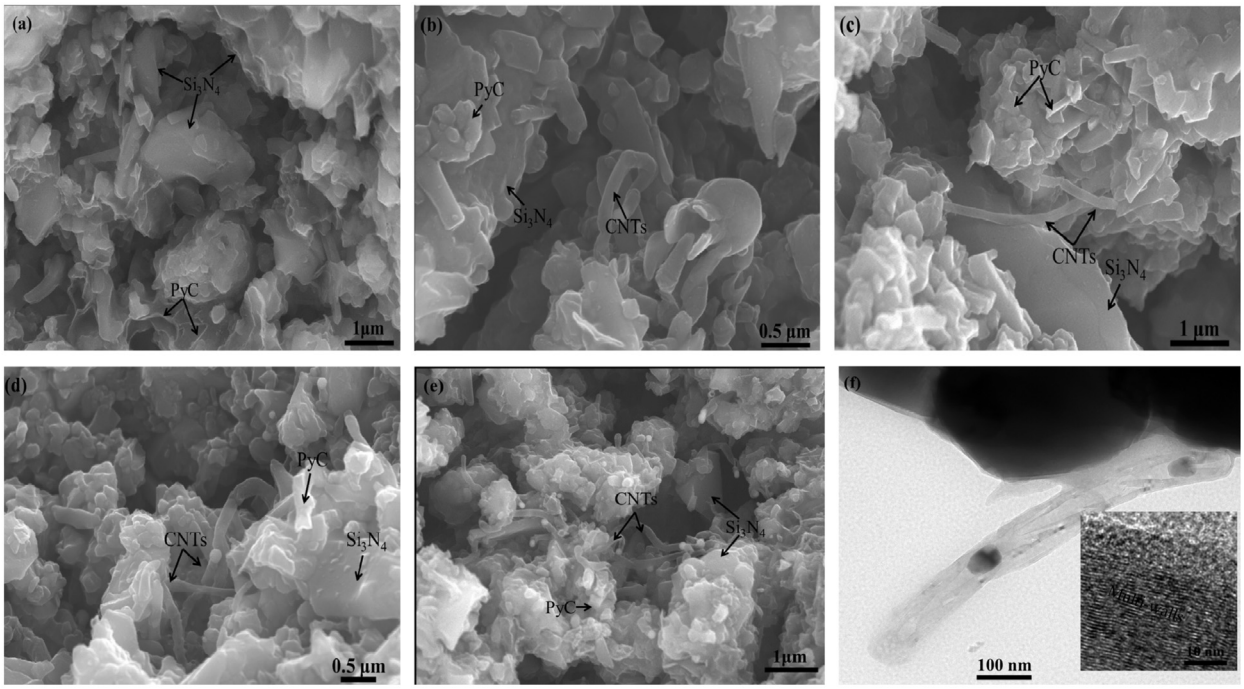

Fig. 6. SEM and TEM images, SEM images of ceramic samples A, B, C, D and E derived from pyrolysis of green bodies with phenolic resin containing 0 wt% (a), 0.25 wt% (b), 0.50 wt% (c), 0.75 wt% (d) and 1.25 wt% (e) Ni catalyst, (f) TEM image of a single CNT, in which inset shows the HRTEM image of CNT.

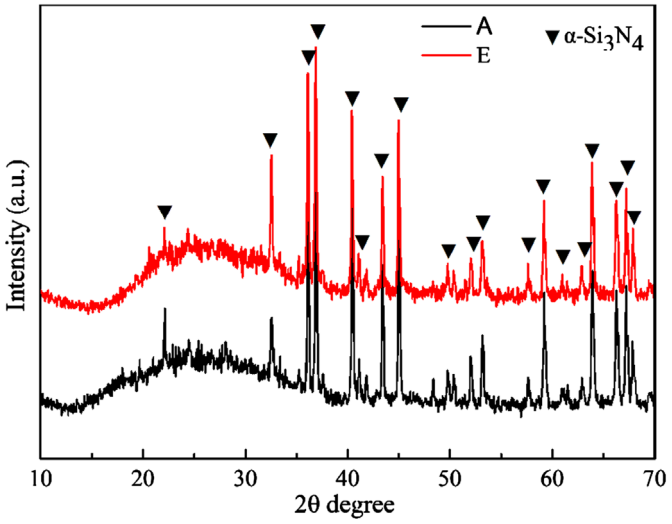

Fig. 7. XRD patterns of PyC–Si_3N_4 (sample A) and CNTs/PyC–Si_3N_4 (sample E) ceramics.

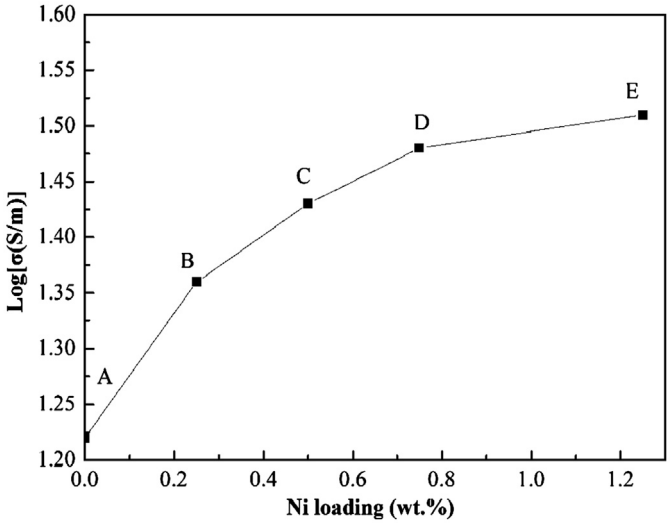

Fig. 8. Electrical conductivity of samples A, B, C, D and E as a function of Ni loading.

Table 3
Si_3N_4, PyC, CNTs and Ni content, porosity and density of PyC–Si_3N_4 and CNTs/PyC–Si_3N_4 ceramics (samples A–E).

Sample	Si_3N_4 content (wt%)	PyC content (wt%)	CNT content (wt%)	Ni content (wt%)	Porosity (vol%)	Density (g/cm^3)
A	83.10	16.90	0	0	42.70	1.67
B	82.50	16.85	0.56	0.09	42.03	1.69
C	81.65	16.74	1.43	0.18	41.16	1.70
D	80.51	16.38	2.86	0.25	40.02	1.72
E	80.30	16.33	2.94	0.43	39.41	1.73

and the values of SE_T increased with the increase of Ni content. To exclude the influence of Ni content on SE_T of PyC–Si_3N_4 ceramics containing different contents of Ni catalyst, the mean values of SE_T and the complex permitivity of 0–1.25 wt% Ni contained paraffin samples were measured (Table 4). The SE_T and the complex permitivity of Ni/paraffin samples were found to be constant with the variation of Ni content, which were attributed to the low content of Ni. Therefore, the increase in SE_T of samples B, C, D and E was ascribed to the contribution of CNTs, which leads to the increase in SE_T from 25.5 dB to 43.6 dB.

Fig. 10(b) shows that SE_A increased with the increasing CNT content. The increase in absorption by increasing CNT concentration is a well-established concept which can be ascribed to higher amount of mobile charge carriers at higher MWCNT concentrations [38–40]. Additionally, the connectivity of CNTs in CNTs/PyC–Si_3N_4 could also contribute to the shielding by absorption [41].

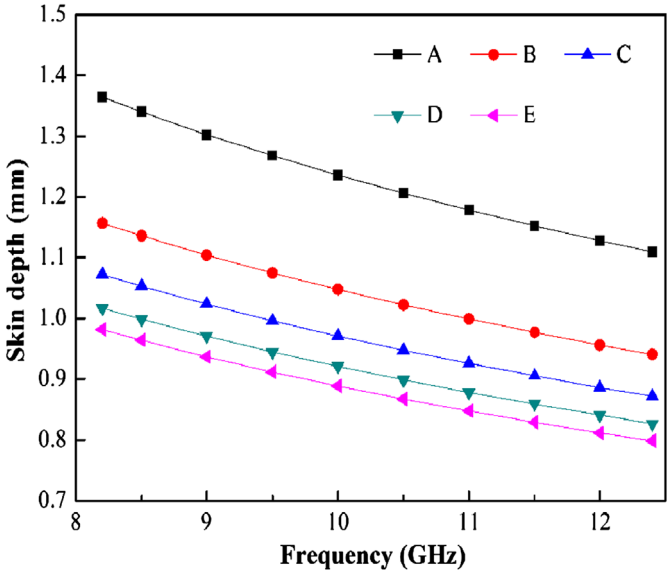

Fig. 9. Skin depth of samples A, B, C, D and E as a function of frequency.

For shielding by reflection, the material should have mobile charge carriers (electrons or holes) to interact with incident electromagnetic wave [39]. In Fig. 10(c), the shielding by reflection increased with the increase in CNT content, which can be related to higher amount of mobile charge carriers at greater MWCNT concentrations. As there is a direct relationship between electrical conductivity and shielding by reflection in conductive monolithic materials [35,37], a higher SE_R is expected in high-concentration CNT contained samples.

3.5. Experimental results versus theoretical predications of EMI SE

Theoretically, the EMI SE of shielding materials can be calculated through the following equations [35,36]:

$$SE_T = SE_R + SE_A + SE_{MR} \tag{7}$$

$$SE_R = 39.5 + 10\log\frac{\sigma}{2\pi f\mu} \tag{8}$$

$$SE_A = 8.7\frac{d}{\delta} = 8.7d\sqrt{\pi f\mu\sigma} \tag{9}$$

$$SE_{MR} = 20\log|1-e^{-2d/\delta}| \tag{10}$$

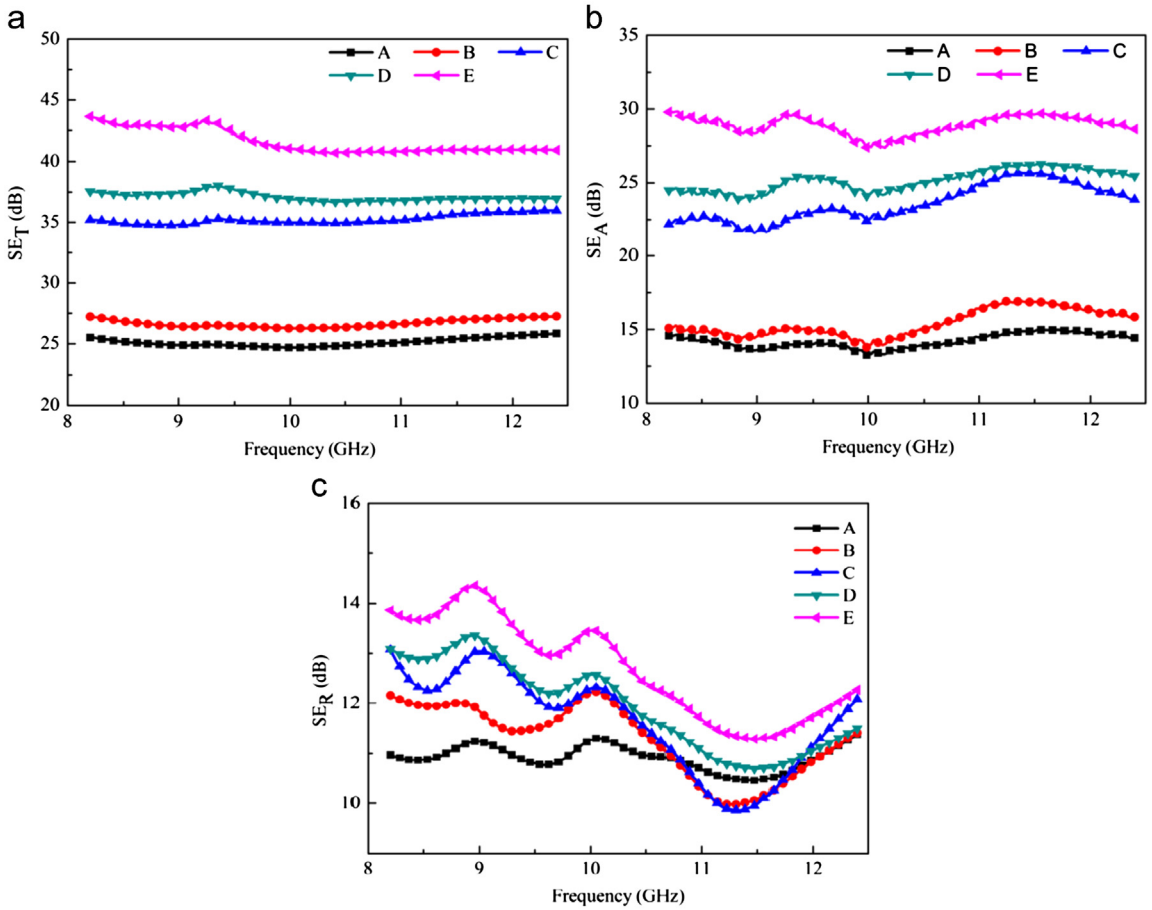

Fig. 10. EMI SE of PyC–Si_3N_4 and CNTs/PyC–Si_3N_4 ceramics, (a) SE_T, (b) SE_A and (c) SE_R of samples A, B, C, D and E as a function of frequency.

Table 4
The mean values of SE_T and complex permittivity of Ni/paraffin specimens containing 0–1.25 wt% Ni contents.

Paraffin content (wt%)	Ni content (wt%)	Real permittivity	Imaginary permittivity	SE_T (dB)
100	0.00	2.2	4.3×10^{-2}	1.0
99.75	0.25	2.2	3.9×10^{-2}	1.0
99.50	0.50	2.2	2.8×10^{-2}	1.0
99.25	0.75	2.2	3.2×10^{-2}	1.0
98.75	1.25	2.2	4.0×10^{-2}	1.0

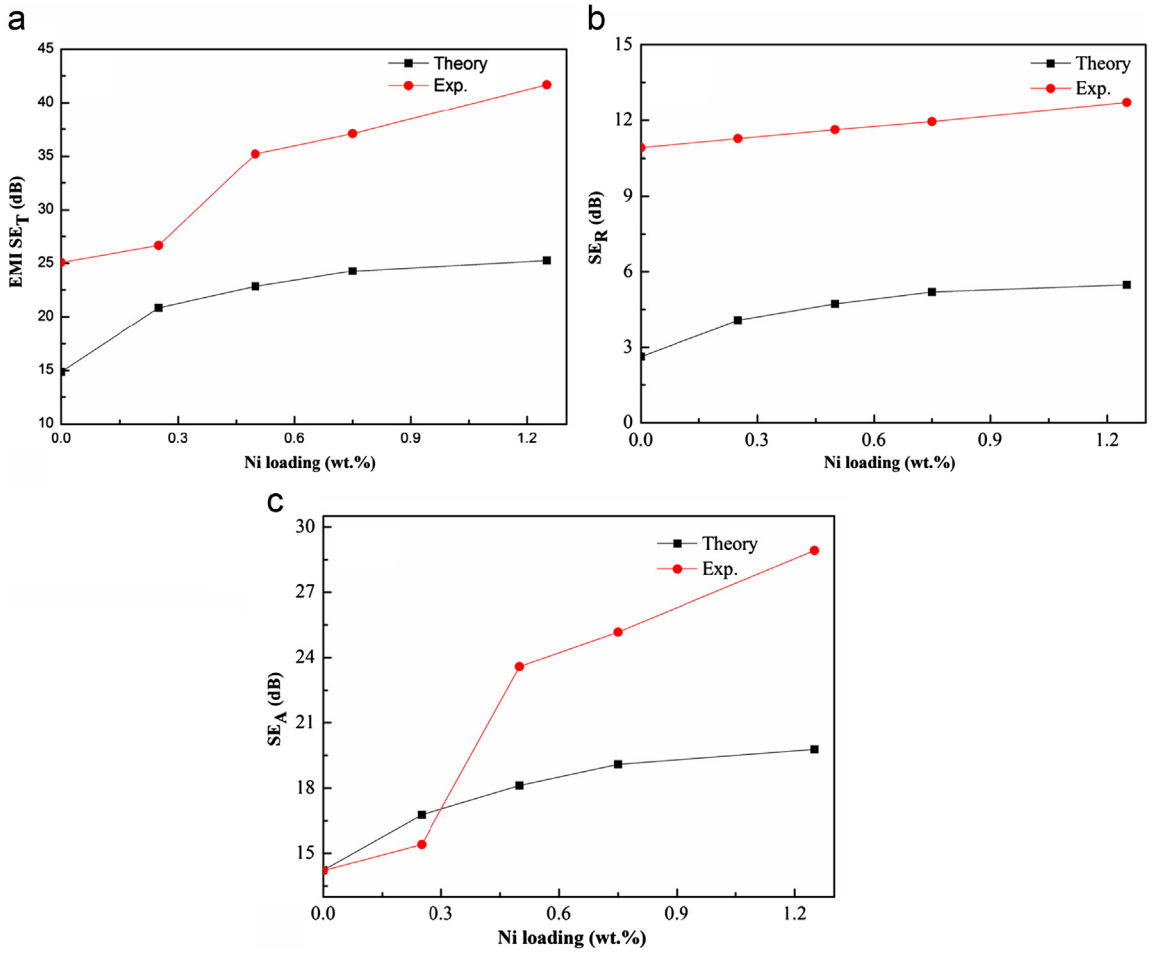

Fig. 11. Average values of EMI SE, (a) SE_T, (b) SE_R and (c) SE_A of samples A, B, C, D and E, experimentally obtained values versus theoretically calculated values as a function of Ni loading.

where SE_{MR} is the shielding by multiple reflections. The calculation of the EMI SE from the above equations is according to the sample thickness, electrical conductivity, magnetic permeability and the EM radiation frequency. When SE_A is higher than 10 dB and the sample thickness is larger than the skin depth, SE_{MR} is always ignored [35,37]. In the present work, the mean value of SE_A is higher than 10 dB, and the sample thickness is greater than skin depth, so the theoretical value of EMI SE was calculated using the following equation:

$$SE_T = SE_R + SE_A \quad (11)$$

The above equation was derived from dense single-phase conductive materials, and there may be difference between the theoretical results and the experimental ones when the shielding materials are porous and composed of different phases [41]. The mean theoretical values and the experimental ones of SE as a function of Ni content are presented in Fig. 11. The experimental value of SE_R is obviously higher than the theoretical one, Fig. 11(b), which can be explained by the larger surface area of porous material than that of dense material [42]. The formation of CNTs in the pores could also increase the surface area. A larger surface area of conductive material could lead to a larger reflection of incident

electromagnetic wave, which leads to a higher SE_R. In Fig. 11(c), the difference between experimental and theoretical values of SE_A increased with the increase of CNT content. This difference may come from the formation of nano-interface between CNTs and PyC which could lead to a strong interfacial polarization relaxation loss, and consequently favors the absorption of microwave [43]. With the increase of CNT content, the interfacial polarization relaxation loss increased gradually and the difference increased at the same time.

4. Conclusion

CNTs were in-situ formed in CNTs/PyC–Si_3N_4 ceramics with the addition of nano-sized Ni particles. The CNT content increased with the increase of Ni loadings. The formation of CNTs in CNTs/PyC leaded to the increase of carbon yield of phenolic resin. Due to the formation of CNTs in the inter-particle pores of CNTs/PyC–Si_3N_4 ceramics, the PyC wrapped Si_3N_4 particles were bridged by CNTs. With increasing CNT content, the electrical conductivity of CNTs/PyC–Si_3N_4 ceramic increased gradually. Composite ceramic exhibited a considerable increase in EMI SE with the increase in the content of CNTs in ceramics. Owing to the contribution of CNTs, SE_T of CNTs/PyC–Si_3N_4 ceramics increased from 25.5 dB to 43.6 dB. Regardless of the electrical conductivity, shielding by absorption was always found to be the major contribution to the total EMI SE. The estimated theoretical overall EMI SE was remarkably lower than the experimental one.

References

[1] B. Fugetsu, E. Sano, M. Sunada, Y. Sambongi, T. Shibuya, X.S. Wang, T. Hiraki, Electrical conductivity and electromagnetic interference shielding efficiency of carbon nanotube/cellulose composite paper, Carbon 46 (2008) 1256–1258.

[2] M.S. Cao, W.L. Song, Z.L. Hou, B. Wen, J. Yuan, The effects of temperature and frequency on the dielectric properties, electromagnetic interference shielding and microwave-absorption of short carbon fiber/silica composites, Carbon 48 (2010) 788–796.

[3] Y.L. Yang, M.C. Gupta, K.L. Dudley, R.W. Lawrence, Novel carbon nanotube-polystyrene foam composites for electromagnetic interference shielding, Nano Lett. 11 (2005) 2131–2134.

[4] Y. Huang, N. Li, Y.F. Ma, D. Feng, F.F. Li, X.B. He, X. Lin, H.J. Gao, Y.S. Chen, The influence of single-walled carbon nanotube structure on the electromagnetic interference shielding efficiency of its epoxy composites, Carbon 45 (2007) 1614–1621.

[5] M.H. Al-Saleh, U. Sundararaj, Electromagnetic interference shielding mechanisms of CNT/Polymer composites, Carbon 47 (2009) 1738–1746.

[6] S.L. Shi, J. Liang, The effect of multi-wall carbon nanotubes on electromagnetic interference shielding of ceramic composites, Nanotechnology 19 (2008) 255707.

[7] M. Rosenow, J. Bell, EMI shielding effectiveness of nickel coated carbon fiber as a long fiber thermoplastic concentrate, in: Proceeding of the 43rd Inter-national SAMPE Symposium, 1998 pp. 854–864.

[8] Z. Osawa, S. Kuwabara, Thermal stability of the shielding effectiveness of composites to electromagnetic interference. Effects of matrix polymers and surface treatment of fillers, Polym. Degrad. Stab. 35 (1992) 33–43.

[9] H. Park, H.E. Kim, K. Niihara, Microstructural evolution and mechanical properties of Si_3N_4 with Yb_2O_3 as a sintering additive, J. Am. Ceram. Soc. 80 (1997) 750–756.

[10] A.J. Pyzik, D.R. Beaman, Microstructure and properties of self-reinforced silicon nitride, J. Am. Ceram. Soc. 76 (1993) 2737–2744.

[11] C. Kawai, A. Yamakawa, Network formation of Si_3N_4 whiskers for the preparation of membrane filters, J. Mater. Sci. Lett. 17 (1998) 873–875.

[12] P.F. Becher, E.Y. Sun, K.P. Plucknett, K.B. Alexander, C.H. Hsueh, H. T. Lin, Microstructure design of silicon nitride with improved fracture toughness: I. Effects of grain shape and size, J. Am. Ceram. Soc. 81 (1998) 2821–2830.

[13] F.L. Riley, Silicon nitride and related materials, J. Am. Ceram. Soc. 83 (2000) 245–265.

[14] J.S. Im, J.G. Kim, Y.S. Lee, Fluorination effects of carbon black additives for electrical proper ties and EMI shielding efficiency by improved dispersion and adhesion, Carbon 47 (2009) 2640–2647.

[15] X.M. Li, L.T. Zhang, X.W. Yin, Synthesis and electromagnetic shielding property of pyrolytic carbon-silicon nitride ceramics with dense silicon nitride coating, J. Am. Ceram. Soc. 95 (2012) 1038–1041.

[16] X. Hao, X.W. Yin, L.T. Zhang, L.F. Cheng, Dielectric, electromagnetic interference shielding and absorption properties of Si_3N_4–PyC composite ceramics, J. Mater. Sci. Technol. 29 (2013) 249–254.

[17] D. Markham, Shielding: quantifying the shielding requirements for portable electronic design and providing new solutions by using a combination of materials and design, Mater. Des. 21 (2000) 45–50.

[18] Z.F. Liu, G. Bai, Y. Huang, Y.F. Ma, F. Du, F.F. Li, T.Y. Guo, Y.S. Chen, Reflection and absorption contributions to the electromagnetic interference shielding of single-walled carbon nanotube/polyurethane composites, Carbon 45 (2007) 821–827.

[19] A. Mohammad, A. Thomas, O. Michal, S. Uttandaraman, Comparative study of electromagnetic interference shielding properties of injection molded versus compression molded multi-walled carbon nanotube/polystyrene composites, Carbon 50 (2012) 5126–5134.

[20] Y. Huang, N. Li, Y.F. Ma, F. Du, F.F. Li, X.B. He, X. Lin, H.J. Gao, Y.S. Chen, The influence of single-walled carbon nanotube structure on the electromagnetic interference shielding efficiency of its epoxy composites, Carbon 45 (2007) 1614–1621.

[21] C. Balazsi, B. Fenyi, N. Hegman, Z. Kover, F. Weber, Z. Vertesy, Z. Konya, I. Kiricsi, L.P. Biro, P. Arato, Development of CNT/Si_3N_4 composites with improved mechanical and electrical properties, Compos. Part B 37 (2006) 418–424.

[22] E. Fitzer, W. Schaefer, S. Yamada, The formation of glasslike carbon by pyrolysis of polyfurfuryl alcohol and phenolic resin, Carbon 7 (1969) 643–646.

[23] Z.P. Zhu, Y. Lu, D.H. Qiao, S. Bai, T.P. Hu, L. Li, J.F. Zheng, Self-catalytic behavior of carbon nanotubes, J. Am. Chem. Soc. 127 (2005) 15698–15699.

[24] G.X. Du, S.A. Feng, J.H. Zhao, C. Song, S. Bai, Z.P. Zhu, Particle-wire-tube mechanism for carbon nanotube evolution, J. Am. Chem. Soc. 128 (2006) 15405–15414.

[25] U.S. Choi, B.G. Ahn, O.K. Kwon, Y.J. Chun, Tribological behavior of some antiwear additives in vegetable oils, Tribol. Int. 30 (1997) 677–683.

[26] Y. Matsumura, M. Okumura, Y. Usami, K. Kagawa, H. Yamashita, M. Anpo, M. Haruta, Low-temperature decomposition of methanol to carbon monoxide and hydrogen with low activation energy over Pd/ZrO_2 catalyst, Catal. Lett. 44 (1997) 189–191.

[27] M. Kumar, Carbon nanotube synthesis and growth mechanism, Nanotechnol. Nanomater. (2011).

[28] L.J. Ci, B.Q. Wei, C.L. Xu, L. Ji, D.H. Wu, S.S. Xie, W.Y. Zhou, Y.B. Li, Z.Q. Liu, D.S. Tan, Crystallization behavior of the amorphous carbon nanotubes prepared by the CVD method, J. Cryst. Growth 233 (2001) 823–828.

[29] J. Abrahamson, The surface energies of graphite, Carbon 11 (1973) 337–362.

[30] H. Hu, C.J. Peng, S.B. Krupanidhi, Effect of heating rate on the crystallization behavior of amorphous PZT thin films, Thin Solid Films 223 (1993) 327–333.

[31] R. Andrews, D. Jacques, D. Qian, E.C. Dickey, Purification and structural annealing of multi-walled carbon nanotubes at graphitization temperatures, Carbon 39 (2001) 1681–1687.

[32] E. Minoux, O. Groening, K.B.K. Teo, S.H. Dalal, L. Gangloff, J.P. Schnell, L. Hudanski, I.Y.Y. Bu, P. Vincent, P. Legagneux, G.A. J. Amaratunga, W.I. Milne, Achieving high-current carbon nanotube emitters, Nano Lett. 11 (2005) 2135–2138.
[33] Z.Q. Guo, G. Blugan, T. Graule, M. Reece, J. Kuebler, The effect of different sintering additives on the electrical and oxidation properties of Si_3N_4–$MoSi_2$ composites, J. Eur. Ceram. Soc. 27 (2007) 2153–2161.
[34] J.J. Hauser, Electrical, structural and optical properties of amorphous carbon, J. Non-Cryst, Solids 23 (1977) 21–41.
[35] K.L. Kaiser, Electromagnetic Shielding, CRC Press, Boca Raton, United States1–52.
[36] P.S. Neelakanta, Handbook of Electromagnetic Materials: Monolithic and Composite Versions and their Applications, CRC Press, Boca Raton, 1995.
[37] C.R. Paul, in: Introduction to Electromagnetic Compatibility, second edition, Wiley, Hoboken, NJ, 2006.
[38] D.D.L. Chung, Materials for electromagnetic interference shielding, J. Mater. Eng. Perform. 9 (2000) 350–354.
[39] M.H. Al-Saleh, U. Sundararaj, Electromagnetic interference shielding mechanisms of CNT/polymer composites, Carbon 47 (2009) 1738–1746.
[40] W.S. Jou, H.Z. Cheng, C.F. Hsu, The electromagnetic shielding effectiveness of carbon nanotubes polymer composites, J. Alloys Compd. 434–435 (2007) 641–645.
[41] M.H. Al-Saleh, U. Sundararaj, X-band EMI shielding mechanisms and shielding effectiveness of high structure carbon black/polypropylene composites, J. Phys. D: Appl. Phys. 46 (2013) 035304.
[42] M. Arjmand, T. Apperley, M. Okoniewski, U. Sundararaj, Comparative study of electromagnetic interference shielding properties of injection molded versus compression molded multi-walled carbon nanotube/polystyrene composites, Carbon 50 (2012) 5126–5134.
[43] X.W. Yin, Y.Y. Xue, L.T. Zhang, L.F. Cheng, Dielectric, electromagnetic absorption and interference shielding properties of porous yttria-stabilized zirconia/silicon carbide composites, Ceram. Int. 38 (2012) 2421–2427.